

## Thin-Film Radiative Thermal Diode with Large Rectification

Qizhang Li<sup>1,2,†</sup>, Haiyu He<sup>1,3,‡</sup>, Qun Chen<sup>2,\*</sup>, and Bai Song<sup>1,3,4,†</sup>

<sup>1</sup>*Beijing Innovation Center for Engineering Science and Advanced Technology, Peking University, Beijing 100871, China*

<sup>2</sup>*Key Laboratory for Thermal Science and Power Engineering of Ministry of Education, Department of Engineering Mechanics, Tsinghua University, Beijing 100084, China*

<sup>3</sup>*Department of Energy and Resources Engineering, Peking University, Beijing 100871, China*

<sup>4</sup>*Department of Advanced Manufacturing and Robotics, Peking University, Beijing 100871, China*

(Received 1 November 2020; revised 2 July 2021; accepted 9 July 2021; published 30 July 2021)

We propose a mechanism to substantially rectify radiative heat flow by having one side of the thermal diode offering a large contrast in the local density of electromagnetic states, while the opposite side serving as a narrow bandpass filter that limits the transport to a desired spectral range. To demonstrate, we realize such a scenario by matching thin films of metal-to-insulator transition materials and polar dielectrics in the near field. By leveraging the distinct scaling behaviors of the local density of states with film thickness for metals and insulators, we theoretically achieve rectification ratios over 140, a 10-fold improvement over the state of the art, with nanofilms of vanadium dioxide and cubic boron nitride in the parallel-plane geometry at experimentally feasible gap sizes ( $\sim 100$  nm). Our rational design offers relative ease of fabrication, flexible choice of materials, and robustness against deviations from optimal film thicknesses. We expect this work to facilitate the application of thermal diodes in solid-state thermal circuits and energy-conversion devices.

DOI: 10.1103/PhysRevApplied.16.014069

### I. INTRODUCTION

Thermal diodes, in analogy to electrical diodes, are two-terminal devices that rectify the flow of heat and are desired in many applications, including thermal management, energy conversion, and thermal circuits and computing [1–3]. The key figure of merit for a thermal diode is its rectification ratio, defined as  $R = (Q_F - Q_R)/Q_R$ , where  $Q_F$  denotes the larger heat current under a forward temperature bias and  $Q_R$  is the smaller reverse current [4]. A 10-fold rectification is often necessary for technical efficiency. However, despite extensive studies of thermal diodes mediated by phonons, electrons, and photons, most experimentally demonstrated rectification ratios remain around one or much smaller [4–8]. With potential for orders-of-magnitude rectification over a wide range of temperatures, near-field radiative thermal diodes (NFRTDs), leveraging the large electromagnetic local density of states (LDOS) close to a surface, have recently gained broad interest [7,9–21].

Research on NFRTDs began with bulk materials in the parallel-plane geometry separated by a vacuum gap. By

using the temperature-dependent surface phonon polaritons (SPhPs) in two polymorphs of silicon carbide (SiC), Otey *et al.* [9] obtained a rectification ratio of 0.41 at a gap size of 100 nm. Subsequently, the surface modes supported by doped semiconductors [10,18], phase-change materials [11,12,15], polar dielectrics [14,17], and two-dimensional materials [16,20] were widely explored, together with nanoscale structural innovations (e.g., multilayers and linear gratings), leading sometimes to rectifications over 10. By using nanospheres instead of parallel planes, the largest rectification, to date ( $> 10^4$ ), has been theoretically predicted [13,19]. However, experiments on NFRTDs are rare and have only reported rectifications around one [7], largely due to challenges in achieving 10-nm gaps between parallel planes and in characterizing radiative thermal transport between delicate nanostructures.

Here, we propose that large rectification of radiative heat flow can be readily achieved by matching and optimizing a thin film of metal-to-insulator transition (MIT) materials and another of polar dielectrics in the parallel-plane geometry, which is the most technologically promising, at experimentally feasible gap sizes [Fig. 1(a)]. We begin with an asymptotic analysis of hypothetical materials to illustrate the physical mechanism, followed by rigorous calculations for thermal diodes composed of realistic materials and structures. We show over 140-fold rectification

\*chenqun@tsinghua.edu.cn

†songbai@pku.edu.cn

‡These authors contributed equally to this work.

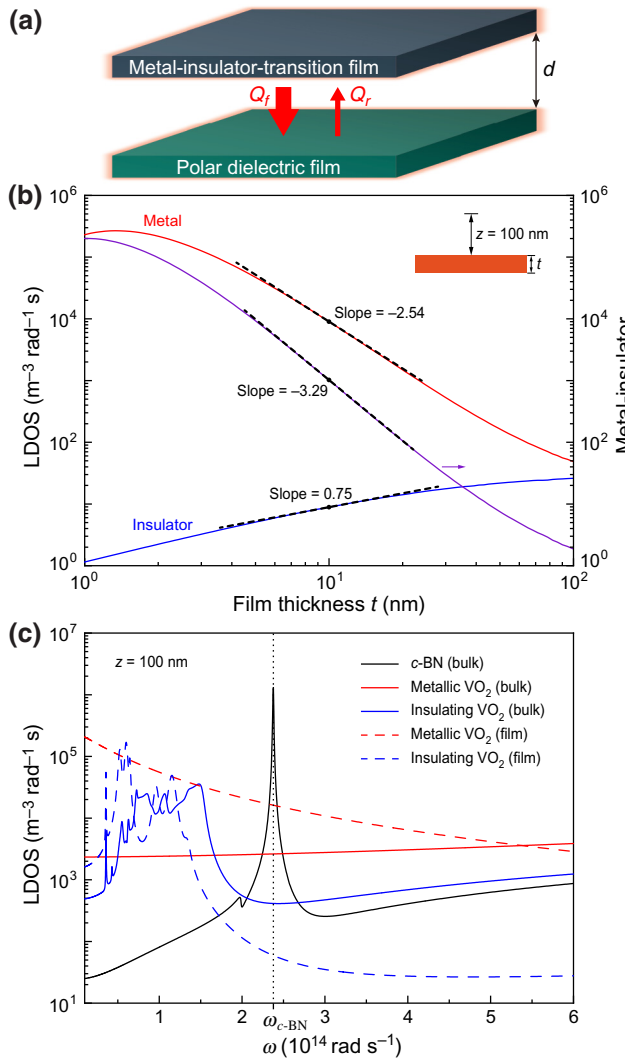


FIG. 1. (a) Schematic of the thin-film radiative thermal diode. (b) LDOS of  $p$ -polarized evanescent modes 100 nm above a metal and an insulator film and their ratio at  $\omega = 10^{14} \text{ rad/s}$  with varying film thickness. For the metal, we assume  $\omega_p = 10\omega$ , so  $\varepsilon'_m \approx 1 - \omega_p^2/\omega^2 = -99$ , and set  $\varepsilon''_m = 10^{-3}$  to represent a low loss. For the insulator, we set  $\varepsilon_i = 2 + 10^{-3}i$ . (c) LDOS above  $c$ -BN and VO<sub>2</sub>.

near room temperature at around 100-nm gaps, together with a high robustness against deviations from optimal film thicknesses. Our results open up the possibility for realizing orders-of-magnitude thermal rectification using state-of-the-art experimental techniques [22–25].

## II. RESULTS AND DISCUSSION

To design a high-performance NFRTD, we first focus on the near-field LDOS because a large LDOS usually leads to a large radiative heat flow and vice versa [26]. Our idea is to create a scenario where one side of the diode offers a substantial LDOS contrast as the temperature varies, while

the other provides a sharp LDOS peak which serves as a narrow bandpass filter and limits the heat flow to a desired frequency range for ease of control. Such a scenario can be established, for example (Fig. 1), by exploring the phase transitions of MIT materials [27] in conjunction with the SPhPs supported by polar dielectrics [28–30].

The key to maximizing rectification is to maximize the contrast of near-field LDOS across the metal-to-insulator transition. We achieve this by simply using a MIT thin film instead of a bulk, because the low-frequency LDOS of a metal film increases substantially with decreasing film thickness while the opposite often happens for an insulator film, as shown in Figs. 1(b) and 1(c). Intuitively, as the thickness of a metal film becomes thinner than the skin depth, the surface plasmon polaritons (SPPs) at the two interfaces couple within the film and split into two branches of resonant modes—the low-frequency symmetric and the high-frequency antisymmetric modes [31,32]. Compared to the SPPs on a bulk material, the symmetric modes of a thin film shift to higher parallel wavevectors and lead to enhanced LDOS that are thermally accessible [32]. On the contrary, the LDOS for an insulator may decrease over a wide frequency range due to reduced emitting volume as the film thickness decreases [33].

To quantify the effect of film thickness on the LDOS contrast, we derive approximate expressions in the near field of both metals and insulators, assuming nonmagnetic materials so only  $p$ -polarized surface modes exist. For  $p$ -polarized evanescent waves, the LDOS at a distance  $z$  above a suspended film of thickness  $t$  is given by [26]

$$\rho(\omega, z) = \int_{k_0}^{\infty} \rho_w(\kappa, \omega, z) d\kappa = \int_{k_0}^{\infty} \frac{\kappa^3}{2\pi^2 \omega |\gamma_0|} e^{-2\text{Im}(\gamma_0)z} \text{Im}(R_f) d\kappa, \quad (1)$$

where  $\rho_w$  denotes the wavevector-resolved local density of states (WLDOS) [34,35],  $\kappa$  is the parallel wavevector,  $k_0 = \omega/c$ ,  $\gamma_0 = \sqrt{k_0^2 - \kappa^2}$ , and  $R_f$  is the reflection coefficient of the film. Since the near-field heat flow is often dominated by high- $\kappa$  modes with  $\kappa \gg k_0$ , the WLDOS can be simplified as

$$\rho_w(\kappa, \omega, z) \approx \frac{1}{2\pi^2 \omega} \kappa^2 e^{-2\kappa z} \text{Im}(R_f). \quad (2)$$

We first consider a film of Drude metal with plasma frequency  $\omega_p$  and negligible loss, the permittivity of which can be written as  $\varepsilon_m = \varepsilon'_m + i\varepsilon''_m$ , where  $\varepsilon'_m \approx 1 - \omega_p^2/\omega^2$  and  $\varepsilon''_m \approx 0$ . By solving for the poles of  $R_f$  at sufficiently low frequencies ( $\omega \ll \omega_p$ ), we find the symmetric resonant modes characterized by  $\kappa_r = 2/(|\varepsilon'_m|t)$  (see the Supplemental Material for details [36]). The increase of  $\kappa_r$  with decreasing film thickness reflects stronger coupling

of SPPs within thinner films [31,32]. Upon resonance we have  $\text{Im}(R_f) = |\varepsilon'_m|/\varepsilon''_m$ , so the WLDOS is written as

$$\rho_{w,m}(\kappa_r, \omega, z) = \frac{2}{\pi^2 \omega \varepsilon''_m |\varepsilon'_m|} e^{-4z/(|\varepsilon'_m|t)} t^{-2}, \quad (3)$$

with a full width at half maximum of  $\Delta\kappa = (4\varepsilon''_m/\varepsilon'^2_m)t^{-1}$ . The LDOS of a metal film can then be approximated by

$$\rho_m \approx \rho_{w,m}(\kappa_r, \omega, z) \Delta\kappa = \frac{8}{\pi^2 \omega |\varepsilon'_m|^3} e^{-4z/(|\varepsilon'_m|t)} t^{-3}, \quad (4)$$

which increases with decreasing film thickness roughly as  $t^{-3}$  and peaks at  $t = 4z/(3|\varepsilon'_m|)$ . Likewise, for an insulator film characterized by  $\varepsilon_i = \varepsilon'_i + i\varepsilon''_i$ , with low loss and no surface modes, the low-frequency LDOS is derived as [36]

$$\rho_i \approx \frac{27\varepsilon''_i(\varepsilon'^2_i + 1)}{16e^3 \pi^2 \omega \varepsilon'^2_i} z^{-4} t. \quad (5)$$

Here, the linear scaling with film thickness reflects the linearly decreasing volume. Equations (4) and (5) show that for a hypothetical MIT film, the LDOS contrast between the metal and the insulator phase could potentially scale as  $t^{-4}$ , in consistency with our intuitive pictures. Further, we plot in Fig. 1(b) rigorously calculated results which agree well with the asymptotic analysis.

Guided by the physical insights from ideal materials, we now explore the potential of real MIT materials for large thermal rectification. To this end, we compute the near-field LDOS for vanadium dioxide ( $\text{VO}_2$ )—a prototypical MIT material with a phase-transition temperature around 341 K [37–39]. As expected, the LDOS of a 1-nm-thick  $\text{VO}_2$  film [38] is up to two orders-of-magnitude larger than that of bulk  $\text{VO}_2$  in the metal phase over a wide spectral range, while a similarly dramatic LDOS decrease is observed in the insulator phase [Fig. 1(c)]. This leads to a substantial increase in the LDOS contrast and forms the basis for large rectification, despite the fact that  $\text{VO}_2$  has non-negligible loss in both phases and fails to quantitatively follow the asymptotic relation with film thickness (Fig. S1) [36]. To form a thermal diode [Fig. 1(a)], we choose cubic boron nitride ( $c\text{-BN}$ ) [40,41] as the polar dielectric that pairs with  $\text{VO}_2$ , because it supports strong SPhPs around  $\omega_{c\text{-BN}} = 2.376 \times 10^{14}$  rad/s, where  $\text{VO}_2$  shows a large metal-to-insulator LDOS ratio [Fig. 1(c)].

With the materials of our NFRTDs selected, we proceed to exact calculations of the forward and reverse heat flows in the parallel-plane configuration. Based on the theoretical framework of fluctuational electrodynamics, the heat flux between two closely spaced bodies across a vacuum gap is

given by [42,43]

$$q(T_1, T_2, d) = \int_0^\infty \frac{d\omega}{4\pi^2} [\Theta(\omega, T_1) - \Theta(\omega, T_2)] \times \int_0^\infty dk \kappa [\tau_s^{12}(\omega, \kappa) + \tau_p^{12}(\omega, \kappa)], \quad (6)$$

where  $\Theta(\omega, T) = \hbar\omega/[\exp(\hbar\omega/k_B T) - 1]$  is the mean energy of a harmonic oscillator less the zero-point contribution at absolute temperature  $T$ ;  $d$  is the gap size; and  $\tau_s^{12}(\omega, \kappa)$  and  $\tau_p^{12}(\omega, \kappa)$  are, respectively, the transmission probabilities for the  $s$ - and  $p$ -polarized modes, which can be expressed in terms of the Fresnel reflection coefficients ( $r$ ) as follows:

$$\tau_{\alpha=s,p}^{12}(\omega, \kappa) = \begin{cases} \frac{(1-|r_\alpha^1|^2)(1-|r_\alpha^2|^2)}{|1-r_\alpha^1 r_\alpha^2 \exp(2i\gamma_0 d)|^2}, & \kappa \leq k_0, \\ \frac{4\text{Im}(r_\alpha^1)\text{Im}(r_\alpha^2)e^{-2\text{Im}(\gamma_0)d}}{|1-r_\alpha^1 r_\alpha^2 \exp(2i\gamma_0 d)|^2}, & \kappa > k_0. \end{cases} \quad (7)$$

In Eq. (7),  $1 - |r_\alpha|^2$  should be replaced with  $1 - |r_\alpha|^2 - |t_\alpha|^2$  for suspended thin films, where  $t_\alpha$  is the transmission coefficient.

We show in Fig. 2 the transmission probabilities for three diode configurations, namely, bulk  $\text{VO}_2$  paired with bulk  $c\text{-BN}$ ,  $\text{VO}_2$  film (10 nm) paired with bulk  $c\text{-BN}$ , and  $\text{VO}_2$  film (10 nm) paired with  $c\text{-BN}$  film (10 nm), at a gap size of 100 nm. The terminal temperatures of the diodes are fixed at  $T_{\text{high}} = 351$  K and  $T_{\text{low}} = 331$  K to allow complete phase transition of  $\text{VO}_2$  [39], which is an isotropic metal at  $T_{\text{high}}$  in the forward scenario and a uniaxial dielectric when the temperature bias is reversed. Compared with the bulk-bulk case [Figs. 2(a)–2(c)], the film-bulk case [Figs. 2(d)–2(f)] shows a larger forward heat flux dominated by the SPhPs within the narrow Reststrahlen band of  $c\text{-BN}$  (Table S1) [36], due to the enhanced low-frequency LDOS of the metallic  $\text{VO}_2$  film [Fig. 1(c)]. While in the reverse scenario, a much smaller heat flux is observed because the reduced volume of insulating  $\text{VO}_2$  leads to smaller contributions from the broadband nonsurface modes with  $\kappa < \text{Re}(\sqrt{\varepsilon_{c\text{-BN}}}) k_0$  (left of the  $c\text{-BN}$  light line in Fig. 2). As a result, a much larger rectification ratio ( $R$ ) of 18.28 is obtained with a  $\text{VO}_2$  film and bulk  $c\text{-BN}$  than that of two bulk layers ( $R = 0.35$ ). Moreover, the rectification ratio increases to 24.31 when bulk  $c\text{-BN}$  is replaced with a thin film [Figs. 2(g)–2(i)], which leads to smaller LDOS outside the Reststrahlen band and weaker coupling with the insulating  $\text{VO}_2$  film. This further reduces the reverse heat flux, while maintaining a large forward flux. As indicated by the parameter  $\eta$  in Table S1 [36], which represents the heat flux mediated by the SPhPs of  $c\text{-BN}$ , creating a scenario characterized by narrowband heat transport is key to achieving large thermal rectification.

By systematically optimizing the film thickness, we predict a maximum rectification of 140.77 by combining

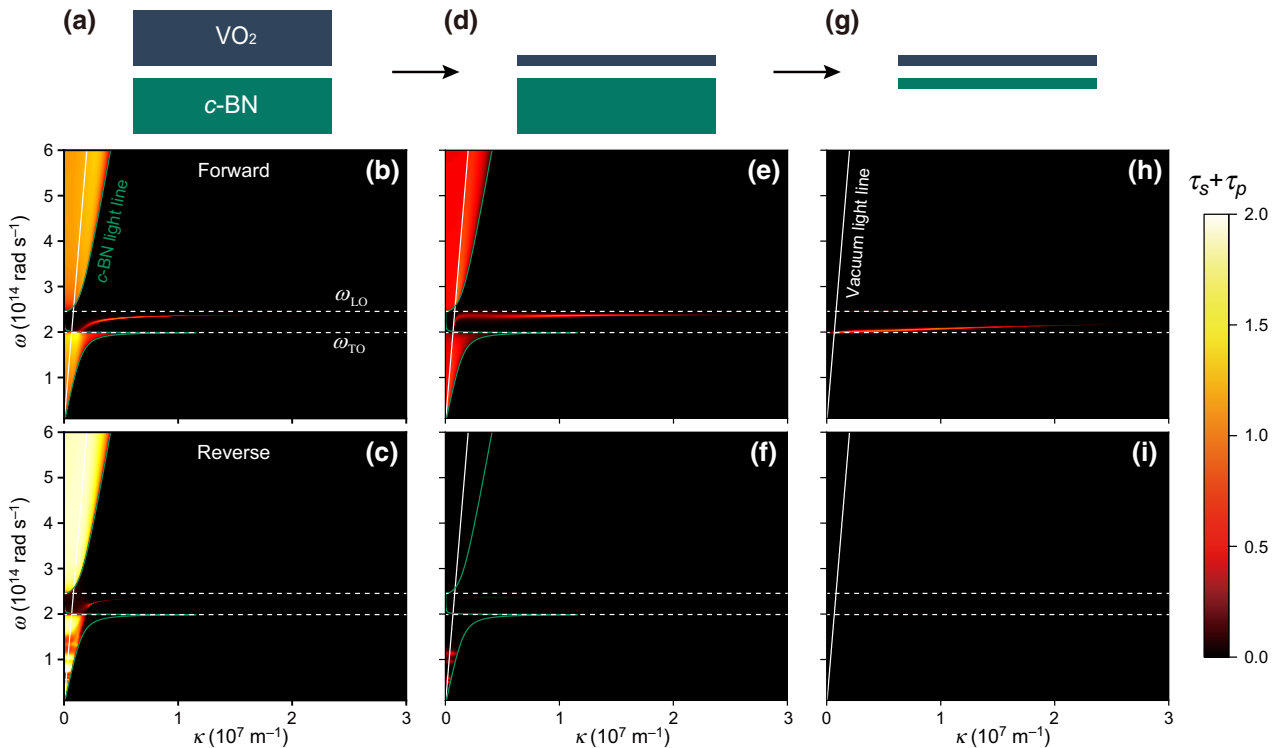


FIG. 2. Comparison of transmission probabilities for bulk and thin-film diodes. (a)–(c) Bulk  $\text{VO}_2$ -bulk  $c\text{-BN}$ , (d)–(f)  $\text{VO}_2$  film-bulk  $c\text{-BN}$ , (g)–(i)  $\text{VO}_2$  film- $c\text{-BN}$  film. Vacuum gap is 100 nm wide, and all films are 10 nm thick. Dashed lines mark the zone-center transverse and longitudinal optical phonons ( $\omega_{\text{TO}}$  and  $\omega_{\text{LO}}$ ) in  $c\text{-BN}$ , which enclose the Reststrahlen band.

a 1-nm-thick  $\text{VO}_2$  film with a 149-nm-thick  $c\text{-BN}$  film (Fig. 3). The dramatic rectification enhancement primarily originates from the ultrathin  $\text{VO}_2$  film, which features a much larger metal-to-insulator LDOS ratio around  $\omega_{c\text{-BN}}$  [Fig. S2(b)] [36], consistent with our asymptotic analysis. In comparison, the optimal  $c\text{-BN}$  film is much thicker. This is because the SPhPs will couple within the  $c\text{-BN}$  film if its thickness becomes smaller than the penetration depth ( $\approx d = 100 \text{ nm}$ ) [30,44,45], leading to a redshift of the LDOS peak to the frequency range where  $\text{VO}_2$  shows a smaller LDOS contrast which reduces rectification [Figs. S2(b) and 2(d)] [36]. We also note that, when the  $\text{VO}_2$  film is around 1 nm thick, the rectification ratio remains above 90, regardless of the  $c\text{-BN}$  film thickness, which again reflects the key role of the ultrathin  $\text{VO}_2$  film [Fig. 3 and Fig. S2(c)] [36].

A thermal diode composed of two suspended nanofilms is theoretically appealing but technically challenging. Here, we build upon the optimized suspended-film design and propose a more practical multilayer structure with similarly large rectification ratio (Fig. 4). First, we add to each film a bulk dielectric substrate with a permittivity,  $\varepsilon_d$ , close to that of vacuum. By setting  $\varepsilon_d = 1 + 10^{-4}i$ , we obtain a rectification of 4.40 across a vacuum gap of 100 nm, in contrast to 140.77 for the suspended-film configuration with the same film thicknesses. This is because of the large reverse heat flux dominated by the broadband

propagating modes in the dielectric substrates with  $\kappa < \text{Re}(\sqrt{\varepsilon_d}) k_0$ , which can be effectively suppressed by reducing the thickness of the substrates. By using a 1- $\mu\text{m}$ -thick substrate instead of the bulk, we observe essentially the

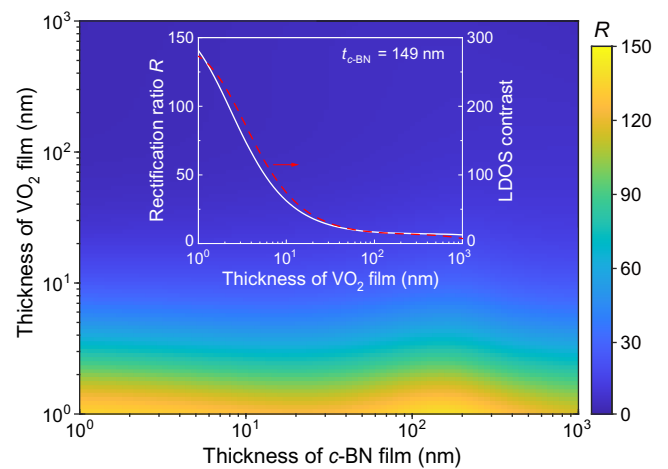


FIG. 3. Rectification ratio of a suspended  $\text{VO}_2$ - $c\text{-BN}$  thin-film diode as a function of film thickness at a 100-nm gap. Inset shows rectification and corresponding LDOS contrast at  $\omega_{c\text{-BN}}$  with varying  $\text{VO}_2$  film thickness, when the  $c\text{-BN}$  film thickness is an optimal value of 149 nm.

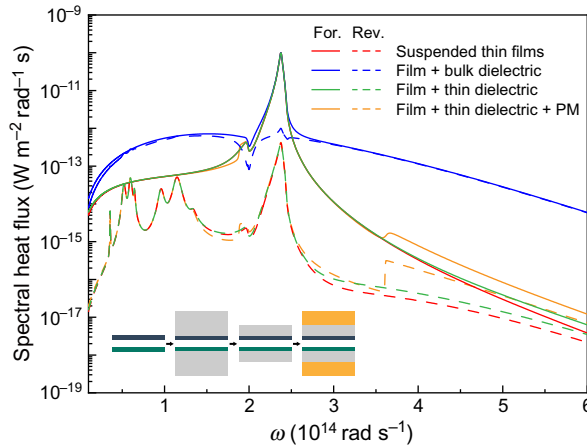


FIG. 4. Spectral heat fluxes of different thin-film diodes in the forward (For.) and reverse (Rev.) scenarios across a 100-nm gap.

same spectral characteristics as those of the suspended-film design and a large rectification ratio of 134.52. We further add a reflective metal layer on the backside of the dielectric substrates to isolate the diode from thermal radiation in the environment. With a perfect metal (PM) [46] as the reflector, the spectrum remains almost unaltered and a rectification ratio of 134.81 is achieved. We note that the dielectric substrate should be thicker than the penetration depth ( $\approx d$ ) of the dominating surface modes ( $\kappa d \approx 1$ ), so that any detrimental effect from the metal reflector is minimized [30,45].

Although the above design is promising, in principle, we have yet to identify real materials that are appropriate to serve as the dielectric substrates and the metal reflectors. The substrates should have vacuumlike permittivities around  $\omega_{c\text{-BN}}$  and should not induce new surface modes, which could increase the reverse heat flow and lower the rectification. We find that potassium chloride (KCl) [47], potassium bromide (KBr) [47], silicon (Si) [48], and SiC [26] represent some of the best candidates. As to the backside reflectors, metals with low loss and high reflectivity, such as silver (Ag) and gold (Au), are preferred. In Fig. 5(a), we present the rectification ratios as a function of gap size for a few thin-film NFRTDs consisting of different combinations of the candidate materials. All of the diodes feature rectification ratios over 60 at a gap size of 100 nm (Table S2) [36], with a maximum of 78.85 achieved by the pair of VO<sub>2</sub>/KBr/Ag and c-BN/SiC/Ag. The rectification ratio of this particular diode further increases to 105.68 at a 50-nm gap, which is readily accessible in the parallel-plane geometry [22,23], and remains greater than 10 even at gap sizes up to about 700 nm. We note that the smaller rectification at larger gaps is due to the rapid decay of the surface modes, while, at smaller gaps, the gap-size-dependent penetration depth of the surface modes is responsible. Indeed, thin films can act like bulk materials in the extreme near

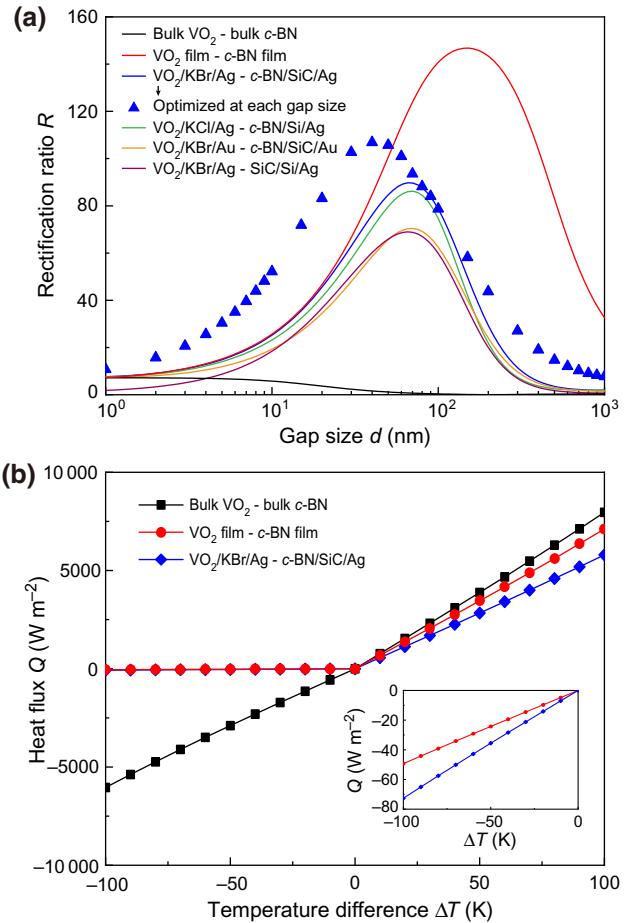


FIG. 5. Performance of optimized thin-film diodes with realistic structures and materials. (a) Gap-dependent rectification ratios. (b) Heat fluxes under different temperature biases at a gap of 100 nm. Terminal temperatures are set as  $T_1 = T_{av} + \Delta T$  and  $T_2 = T_{av} - \Delta T$ , respectively, for the VO<sub>2</sub> and the c-BN sides, with  $T_{av}$  fixed at 341 K, which is the nominal phase-transition temperature of VO<sub>2</sub>.

field and results in rectification ratios approaching the bulk-bulk case [30,45,49]. Last but not least, our thin-film diodes are expected to perform well over a wide temperature range [Fig. 5(b)] and against inevitable film thickness variations in fabrication (Fig. S3) [36].

### III. CONCLUSIONS

We propose a mechanism to achieve orders-of-magnitude rectification of radiative heat flow between parallel planes across experimentally attainable vacuum gaps. We combine an ultrathin MIT film with a polar dielectric film, so that the latter enables surface-mode-mediated narrowband heat transport over a spectral range where the former provides a large metal-to-insulator LDOS contrast upon phase transition. Our asymptotic analysis reveals that the LDOS ratio could increase with decreasing film thickness ( $t$ ) as  $t^{-4}$ , leading to a similarly dramatic rectification

enhancement. We demonstrate a rectification ratio of over 140 by pairing thin films of VO<sub>2</sub> and *c*-BN at a gap size of 100 nm, which is 400 times better than its bulk counterpart and a 10-fold improvement over state-of-the-art thermal diodes. We further explore realistic multilayer structures and identify a variety of appropriate materials. Our effort paves the way for the long-awaited use of thermal diodes in solid-state energy and logic devices.

## ACKNOWLEDGMENTS

This work is supported by the National Natural Science Foundation of China (Grants No. 52076002 and No. 51836004), the Beijing Innovation Center for Engineering Science and Advanced Technology (BIC-ESAT), the XPLORER PRIZE from the Tencent Foundation, and the High-performance Computing Platform of Peking University.

- 
- [1] N. Li, J. Ren, L. Wang, G. Zhang, P. Hänggi, and B. Li, Colloquium: Phononics: Manipulating heat flow with electronic analogs and beyond, *Rev. Mod. Phys.* **84**, 1045 (2012).
  - [2] A. A. Maznev, A. G. Every, and O. B. Wright, Reciprocity in reflection and transmission: What is a ‘phonon diode’?, *Wave Motion* **50**, 776 (2013).
  - [3] G. Wehmeyer, T. Yabuki, C. Monachon, J. Wu, and C. Dames, Thermal diodes, regulators, and switches: Physical mechanisms and potential applications, *Appl. Phys. Rev.* **4**, 41304 (2017).
  - [4] C. W. Chang, D. Okawa, A. Majumdar, and A. Zettl, Solid-state thermal rectifier, *Science* **314**, 1121 (2006).
  - [5] M. J. Martínez-Pérez, A. Fornieri, and F. Giazotto, Rectification of electronic heat current by a hybrid thermal diode, *Nat. Nanotechnol.* **10**, 303 (2015).
  - [6] H. Wang, S. Hu, K. Takahashi, X. Zhang, H. Takamatsu, and J. Chen, Experimental study of thermal rectification in suspended monolayer graphene, *Nat. Commun.* **8**, 15843 (2017).
  - [7] A. Fiorino, D. Thompson, L. Zhu, R. Mittapally, S.-A. Biehs, O. Bezencenet, N. El-Bondy, S. Bansropun, P. Ben-Abdallah, E. Meyhofer, and P. Reddy, A thermal diode based on nanoscale thermal radiation, *ACS Nano* **12**, 5774 (2018).
  - [8] M. Kasprzak, M. Sledzinska, K. Zaleski, I. Iatsunskyi, F. Alzina, S. Volz, C. M. Sotomayor Torres, and B. Graczykowski, High-temperature silicon thermal diode and switch, *Nano Energy* **78**, 105261 (2020).
  - [9] C. R. Otey, W. T. Lau, and S. Fan, Thermal Rectification Through Vacuum, *Phys. Rev. Lett.* **104**, 154301 (2010).
  - [10] S. Basu and M. Francoeur, Near-field radiative transfer based thermal rectification using doped silicon, *Appl. Phys. Lett.* **98**, 113106 (2011).
  - [11] Y. Yang, S. Basu, and L. Wang, Radiation-based near-field thermal rectification with phase transition materials, *Appl. Phys. Lett.* **103**, 163101 (2013).
  - [12] J. Huang, Q. Li, Z. Zheng, and Y. Xuan, Thermal rectification based on thermochromic materials, *Int. J. Heat Mass Transf.* **67**, 575 (2013).
  - [13] L. Zhu, C. R. Otey, and S. Fan, Ultrahigh-contrast and large-bandwidth thermal rectification in near-field electromagnetic thermal transfer between nanoparticles, *Phys. Rev. B* **88**, 184301 (2013).
  - [14] K. Joulain, Y. Ezzahri, J. Drevillon, B. Rousseau, and D. De Sousa Meneses, Radiative thermal rectification between SiC and SiO<sub>2</sub>, *Opt. Express* **23**, A1388 (2015).
  - [15] A. Ghanekar, J. Ji, and Y. Zheng, High-rectification near-field thermal diode using phase change periodic nanostructure, *Appl. Phys. Lett.* **109**, 123106 (2016).
  - [16] Z. Zheng, X. Liu, A. Wang, and Y. Xuan, Graphene-assisted near-field radiative thermal rectifier based on phase transition of vanadium dioxide (VO<sub>2</sub>), *Int. J. Heat Mass Transf.* **109**, 63 (2017).
  - [17] L. Tang and M. Francoeur, Photonic thermal diode enabled by surface polariton coupling in nanostructures, *Opt. Express* **25**, A1043 (2017).
  - [18] J. Shen, X. Liu, H. He, W. Wu, and B. Liu, High-performance noncontact thermal diode via asymmetric nanostructures, *J. Quant. Spectrosc. Radiat. Transf.* **211**, 1 (2018).
  - [19] S. Wen, X. Liu, S. Cheng, Z. Wang, S. Zhang, and C. Dang, Ultrahigh thermal rectification based on near-field thermal radiation between dissimilar nanoparticles, *J. Quant. Spectrosc. Radiat. Transf.* **234**, 1 (2019).
  - [20] Y. Zhang, C. Zhou, H. Yi, and H. Tan, Radiative Thermal Diode Mediated by Nonreciprocal Graphene Plasmon Waveguides, *Phys. Rev. Appl.* **13**, 34021 (2020).
  - [21] A. Ott and S.-A. Biehs, Thermal rectification and spin-spin coupling of nonreciprocal localized and surface modes, *Phys. Rev. B* **101**, 155428 (2020).
  - [22] B. Song, D. Thompson, A. Fiorino, Y. Ganjeh, P. Reddy, and E. Meyhofer, Radiative heat conductances between dielectric and metallic parallel plates with nanoscale gaps, *Nat. Nanotechnol.* **11**, 509 (2016).
  - [23] A. Fiorino, D. Thompson, L. Zhu, B. Song, P. Reddy, and E. Meyhofer, Giant enhancement in radiative heat transfer in sub-30 nm gaps of plane parallel surfaces, *Nano Lett.* **18**, 3711 (2018).
  - [24] M. Ghashami, H. Geng, T. Kim, N. Iacopino, S. K. Cho, and K. Park, Precision Measurement of Phonon-Polaritonic Near-Field Energy Transfer Between Macroscale Planar Structures Under Large Thermal Gradients, *Phys. Rev. Lett.* **120**, 175901 (2018).
  - [25] J. DeSutter, L. Tang, and M. Francoeur, A near-field radiative heat transfer device, *Nat. Nanotechnol.* **14**, 751 (2019).
  - [26] K. Joulain, J.-P. Mulet, F. Marquier, R. Carminati, and J.-J. Greffet, Surface electromagnetic waves thermally excited: Radiative heat transfer, coherence properties and Casimir forces revisited in the near field, *Surf. Sci. Rep.* **57**, 59 (2005).
  - [27] P. J. van Zwol, K. Joulain, P. Ben-Abdallah, and J. Chevrier, Phonon polaritons enhance near-field thermal transfer across the phase transition of VO<sub>2</sub>, *Phys. Rev. B* **84**, 161413 (2011).
  - [28] S. Shen, A. Narayanaswamy, and G. Chen, Surface phonon polaritons mediated energy transfer between nanoscale gaps, *Nano Lett.* **9**, 2909 (2009).

- [29] E. Rousseau, A. Siria, G. Jourdan, S. Volz, F. Comin, J. Chevrier, and J.-J. Greffet, Radiative heat transfer at the nanoscale, *Nat. Photonics* **3**, 514 (2009).
- [30] B. Song, Y. Ganjeh, S. Sadat, D. Thompson, A. Fiorino, V. Fernández-Hurtado, J. Feist, F. J. García-Vidal, J. C. Cuevas, P. Reddy, and E. Meyhofer, Enhancement of near-field radiative heat transfer using polar dielectric thin films, *Nat. Nanotechnol.* **10**, 253 (2015).
- [31] E. N. Economou, Surface plasmons in thin films, *Phys. Rev.* **182**, 539 (1969).
- [32] S.-A. Biehs, Thermal heat radiation, near-field energy density and near-field radiative heat transfer of coated materials, *Eur. Phys. J. B* **58**, 423 (2007).
- [33] M. Francoeur, M. P. Mengüç, and R. Vaillon, Near-field radiative heat transfer enhancement via surface phonon polaritons coupling in thin films, *Appl. Phys. Lett.* **93**, 43109 (2008).
- [34] Y. Guo, C. L. Cortes, S. Molesky, and Z. Jacob, Broad-band super-Planckian thermal emission from hyperbolic metamaterials, *Appl. Phys. Lett.* **101**, 131106 (2012).
- [35] O. D. Miller, S. G. Johnson, and A. W. Rodriguez, Effectiveness of Thin Films in Lieu of Hyperbolic Metamaterials in the Near Field, *Phys. Rev. Lett.* **112**, 157402 (2014).
- [36] See the Supplemental Material at <http://link.aps.org/supplemental/10.1103/PhysRevApplied.16.014069> for derivations of the asymptotic expressions of LDOS, the asymptotic and exact LDOS for real materials, the effect of film thickness on rectification, a Monte Carlo study of diode robustness, and the optimal parameters for different NFRTDs.
- [37] J. Barker, H. Verleur, and H. Guggenheim, Infrared Optical Properties of Vanadium Dioxide Above and Below the Transition Temperature, *Phys. Rev. Lett.* **17**, 1286 (1966).
- [38] H. Paik, J. A. Moyer, T. Spila, J. W. Tashman, J. A. Mundy, E. Freeman, N. Shukla, J. M. Lapano, R. Engel-Herbert, W. Zander, J. Schubert, D. A. Muller, S. Datta, P. Schiffer, and D. G. Schlom, Transport properties of ultra-thin VO<sub>2</sub> films on (001) TiO<sub>2</sub> grown by reactive molecular-beam epitaxy, *Appl. Phys. Lett.* **107**, 163101 (2015).
- [39] S. Lee, K. Hippalgaonkar, F. Yang, J. Hong, C. Ko, J. Suh, K. Liu, K. Wang, J. J. Urban, X. Zhang, C. Dames, S. A. Hartnoll, O. Delaire, and J. Wu, Anomalously low electronic thermal conductivity in metallic vanadium dioxide, *Science* **355**, 371 (2017).
- [40] A. Narayanaswamy and G. Chen, Surface modes for near field thermophotovoltaics, *Appl. Phys. Lett.* **82**, 3544 (2003).
- [41] K. Chen, *et al.*, Ultrahigh thermal conductivity in isotope-enriched cubic boron nitride, *Science* **367**, 555 (2020).
- [42] S.-A. Biehs, E. Rousseau, and J.-J. Greffet, Mesoscopic Description of Radiative Heat Transfer at the Nanoscale, *Phys. Rev. Lett.* **105**, 234301 (2010).
- [43] B. Song, A. Fiorino, E. Meyhofer, and P. Reddy, Near-field radiative thermal transport: From theory to experiment, *AIP Adv.* **5**, 53503 (2015).
- [44] D.-Z. A. Chen, A. Narayanaswamy, and G. Chen, Surface phonon-polariton mediated thermal conductivity enhancement of amorphous thin films, *Phys. Rev. B* **72**, 155435 (2005).
- [45] M. Francoeur, M. P. Mengüç, and R. Vaillon, Coexistence of multiple regimes for near-field thermal radiation between two layers supporting surface phonon polaritons in the infrared, *Phys. Rev. B* **84**, 75436 (2011).
- [46] J. K. Tong, W. C. Hsu, Y. Huang, S. V. Boriskina, and G. Chen, Thin-film “thermal well” emitters and absorbers for high-efficiency thermophotovoltaics, *Sci. Rep.* **5**, 10661 (2015).
- [47] E. D. Palik, *Handbook of Optical Constants of Solids* (Elsevier, New York, 1985).
- [48] C. Fu and Z. Zhang, Nanoscale radiation heat transfer for silicon at different doping levels, *Int. J. Heat Mass Transf.* **49**, 1703 (2006).
- [49] K. Kim, B. Song, V. Fernández-Hurtado, W. Lee, W. Jeong, L. Cui, D. Thompson, J. Feist, M. T. H. Reid, F. J. García-Vidal, J. C. Cuevas, E. Meyhofer, and P. Reddy, Radiative heat transfer in the extreme near field, *Nature* **528**, 387 (2015).